DD

C2

EUROPEAN ORGANIZATION FOR NUCLEAR RESEARCH

CERN/ECP 93–17
12 November 1993
SW 9417

REVERSE ANNEALING OF THE EFFECTIVE IMPURITY CONCENTRATION AND LONG-TERM OPERATIONAL SCENARIO FOR SILICON DETECTORS IN FUTURE COLLIDER EXPERIMENTS

CERN Detector R&D Collaboration RD2

Presented by E. Fretwurst

E. Fretwurst[1)], H. Feick[1)], M. Glaser[2)], C. Gößling[3)], E.H.M. Heijne[2)], A. Hess[1)], F. Lemeilleur[2)], G. Lindström[1)], K.H. Mählmann[1)], A. Rolf[3)], T. Schulz[1)] and C. Soave[2)]

CM-P00049305

Abstract

Systematic investigations of the reverse-annealing effect after radiation damage have been performed in particular for the change of the effective impurity concentration. The pronounced long-term anneal observed at room temperature was investigated further by isochronal and isothermal studies. In order to demonstrate the radiation hardness of silicon detectors during 10 years of LHC operation an experiment was started at a higher temperature which compressed the real operational scenario to about 10 months.

Presented at the International Symposium on Development and Application of Semiconductor Tracking Detectors, Hiroshima, Japan, 22–24 May 1993.

1) Institut für Experimentalphysik und UKE, Universität Hamburg, Germany.
2) CERN, Geneva, Switzerland.
3) Institut für Experimentalphysik IV, Universität Dortmund, Germany.

1 INTRODUCTION

Radiation damage in silicon detectors by fast neutrons and protons results in a change of the effective impurity concentration, an increase of the reverse leakage current, and a degradation of the charge collection efficiency (see for example Refs. [1–7] and the literature cited there). High-intensity irradiations in short exposures are inevitable for these studies since this is the only way that the generation of the primary damage defects can be distinguished from the succeeding annealing processes. With respect to realistic operational scenarios in future collider experiments long-term annealing is of special relevance. In this paper we concentrate on the observed reverse annealing of the effective impurity concentration, since this effect increases the depletion voltage and will, therefore, finally limit the operability of the detectors. In order to gain more insight into the defect dynamics involved we started investigations with different heat treatments, and developed a model describing the dependence on the temperature. Based on these results an experiment was designed, in which the 10-year operational scenario for a typical LHC application was compressed to about 10 months. The first results of this study will also be presented and discussed.

2 EXPERIMENTAL PROCEDURE

Detectors fabricated with high-resistivity float zone n-type silicon (Wacker Chemitronic) were used throughout the experiments. These diodes were manufactured both by ion implantation (Micron Semiconductor Ltd.) and the surface barrier technique (University of Hamburg) in order to ensure that the measured effects do not depend on the individual process technology.

The irradiations were performed at the following facilities:

a) Neutron irradiations at the Physikalisch-Technische-Bundesanstalt Braunschweig (PTB) using the Be(d,n) reaction for the production of a high-intensity neutron beam with a mean energy of 6.2 MeV [8].
b) Neutron irradiations at the irradiation facility of the proton synchrotron at CERN (PSAIF) providing a mean energy of about 1 MeV [9].
c) Neutron irradiations at the University Hospital Hamburg (UKE) using the T(d,n) reaction that delivers 14.1 MeV monoenergetic neutrons [10]. This facility was especially useful for the 10-year compressed scenario in which successive irradiations had to be performed each month.
d) The 24 GeV proton beam of the proton synchrotron at CERN was used directly for the study of p-induced defects.

The particle fluences given in this report are values normalized to an equivalent neutron fluence for 1 MeV. Assuming that the damage effect is only caused by the displacement cross-section, this normalization was carried out via the particle and energy-dependent non-ionizing energy loss (NIEL) (for details see Refs. [3,7]).

The change of the effective impurity concentration measured with standard capacitance voltage techniques was then studied after different treatments. For the study of the isochronal

annealing we used heat cycles of 1 h each and temperature steps of 20°C up to 200°C. The isothermal experiments were carried out maintaining a constant temperature interrupted only by short periods needed for the C/V measurements at room temperature. After irradiation the detectors were first kept at room temperature for a period of 15 days before starting the isothermal heat treatment. This ensured that the normal short-term annealing had almost completely decayed, and only the reverse annealing was observed from then on. Hence, the time scale given in our experimental results starts at the beginning of the heat treatment. As the measured effects depend very much on the temperature it should be mentioned that in most cases the variations were kept within ± 0.5°C.

All of the relevant detector data, the irradiation parameters, and the subsequent heat treatments are listed in Table 1.

3 EXPERIMENTAL RESULTS AND DISCUSSION

Figure 1 demonstrates the reverse-annealing effect at room temperature after neutron irradiation with two different fluences. As in all of the other figures only the change of the effective impurity concentration with respect to the initial value before irradiation is plotted. It can be clearly seen that after a quite strong but short decrease within the first 10 days, a continuous increase is observed. It can also be noted that all irradiations used for these investigations resulted in type inversion, i.e. in the change from the initial n-type to p-type silicon [3]. We assume that the reverse annealing is produced by the transformation of originally electrically-inactive defects into acceptor-like states. Hence, as a first guess, we expect the overall effect to be proportional to the fluence. Disregarding the small difference in the minima for $\Delta N_{eff}/\Phi_{eq}$ this expectation is indeed fulfilled. Both curves have the same time dependence within one year. Similar results were obtained by Gill et al. [6].

The above-mentioned assumption would result in a final saturation of the reverse annealing at a given level. From the room temperature measurements, such a saturation level cannot easily be extracted because of the long reverse-annealing time constant. However, it is possible to accelerate this process by increasing the detector temperature. In order to get more insight into this possibility isochronal annealing studies with 1 h per step were carried out between room temperature and 200°C. As can be seen from Fig. 2, the change of the effective impurity concentration increases steeply between 350 K and 390 K, and then above 420 K. These two steps indicate two different annealing stages centred at about 370 K and 440 K. From a straightforward first-order analysis it can be shown that the 370 K stage is the only one responsible for the reverse annealing at room temperature, and that no interference from the second stage is to be expected as long as the isothermal studies are carried out below 70°C [11].

The first results of these isothermal studies are shown in Fig. 3. The following two assumptions may be used as an explanation (see for example Ref. [12]).

Assumption (A):

Here we assume that the primary defect X responsible for the reverse annealing is electrically inactive. Owing to its successive decay with a characteristic time constant τ, it then forms an electrically active one Y. The rate equation for the concentration N_X is given by

$$dN_X = - 1/\tau \cdot N_X \cdot dt \, . \qquad (1)$$

This results in the well-known exponential decay of N_X, and hence the formation of the final defect Y is governed by

$$N_Y(t) = N_{X,0}\{1 - \exp(-t/\tau)\} . \quad (2)$$

As for the generation of all defects we assume that the initial concentration $N_{X,0}$ is proportional to the fluence Φ. Therefore, N_Y represents only the change of the effective impurity concentration.

Assumption (B):

Another parametrization is achieved by the following second-order approach. In this case we assume a generation of electrically-inactive defects X_1, X_2 which interact with each other forming the electrically-active defect Y. Again $N_{X1,0}$, $N_{X2,0}$ should be proportional to Φ. If one of the defect concentrations should dominate the other one, the description would lead back to the first-order process. Hence, a second-order process can only be expected if $N_{X1,0} \approx N_{X2,0}$. For simplicity we assume $N_{X1,0} = N_{X2,0} = N_{X,0}$. Of course, one possibility for such a situation would be that the induced defects X_1, X_2 are physically identical. The rate equation for this process is then

$$dN_X = -k \cdot N_X^2 \cdot dt . \quad (3)$$

This leads to a decay of the defect concentration N_X, and consequently the formation of the final defect Y according to

$$N_Y(t) = N_{X,0}\{1 - (1 + k \cdot N_{X,0} \cdot t)^{-1}\} . \quad (4)$$

As for the first-order approach, N_Y saturates at the initial concentration $N_{X,0}$, but the time dependence for both cases is different. The product $(k \cdot N_{X,0})$ in Eq. (4) can be used for the definition of a half-life time according to

$$t_{1/2} = (k \cdot N_{X,0})^{-1} . \quad (5)$$

In contrast with the first-order process, $t_{1/2}$ depends on the initial value $N_{X,0}$, and therefore on the radiation fluence.

Neglecting the short-term annealing, we parametrized the time dependence of the total change of the effective impurity concentration at a given annealing temperature T by

$$\Delta N_{eff}(t,T) = N_C(T) + N_Y(t,T) , \quad (6)$$

where t is the accumulated annealing time, and the constant term N_C represents the generation of electrically-active defects which are assumed to remain stable. The resulting first-order fit [Eq. (2)] to the data at different annealing temperatures is then demonstrated by the broken lines in Fig. 3. A much better fit is achieved by the second-order approach [Eq. (4)] which is represented by the solid lines. Therefore, this parametrization was used as a consistent description for all temperatures, and also for additional annealing studies carried out for detectors fabricated by a different process and after proton irradiation (Fig. 4) .

The results of the second-order fits to all measured reverse-annealing functions are summarized in Table 2. It should be mentioned that the extracted parameters for 21°C are mean values derived from different detectors irradiated with neutrons in the range $(3.1–8.7) \times 10^{13}$ n/cm^2 (Table 1). The rate constant k exhibits large fluctuations due to the limited time period of about one year for the measurements after irradiation. This is also true for the measurements presented in Fig. 4 at about 25°C. Nevertheless, the strong temperature dependence of k is obvious. The change is more than two orders of magnitude in the temperature range under investigation. According to Corbett [12] this can be expected if there is a single activation energy involved in the kinetics of the annealing process. In this case the temperature dependence of the rate constant k follows an Arrhenius relation

$$k = k_0 \cdot \exp(- E_a/k_B \cdot T) , \qquad (7)$$

where k_B is the Boltzmann constant, and k_0 a constant which is related to the most abundant phonon frequency in the lattice. In Fig. 5 ln k plotted against 1/T for the values listed in Table 2 is shown. Taking the errors into account a linear fit seems to be reasonable. This would result in an activation energy of $E_a = 1.33 \pm 0.07$ eV.

On the other hand, the reverse-annealing amplitude, with respect to the generation rate $N_{X,0}/\Phi$, is about 0.05 cm^{-1} for neutron- and proton-irradiated samples disregarding the value obtained for the sample M04 which is about a factor of two smaller than given above. The constant term N [Eq. (6)] extracted from the second-order fit is plotted in Fig. 6 as a function Φ_{eq}. Disregarding the values for the Micron detectors this term exhibits a linear dependence on Φ_{eq}. This may indeed be expected using the following arguments: the high fluences used throughout the experiments were always leading to type inversion. This means that the phosphor donors are practically exhausted, for example by forming V–P centres. These complex defects are annealing out only at temperatures above 170°C, i.e. far above the temperature range under investigation. Therefore, the constant term has two components. The first belongs to the total removal of donors remaining independent of Φ after exhaustion, and the second one is related to that part of the generated acceptor-like states which do not anneal. This part is therefore proportional to Φ [7].

Taking the temperature dependence of the generation rate constant k for granted, we would expect at 0°C an extrapolated value of $k = 3.0 \times 10^{-22}$ cm^3/s. This leads to a time constant $t_{1/2} \approx 210$ years, assuming the same value of $N_{X,0}/\Phi$ as mentioned above, and a fluence of 1×10^{13} cm^{-2}. Therefore, reverse annealing should be completely frozen at 0°C. Figure 7 demonstrates the annealing behaviour of a neutron-irradiated detector at 0°C compared with a 20°C case. After a short-term anneal, $\Delta N_{eff}/\Phi$ stays constant over a period of about 150 days at a level of 0.045 cm^{-1}. Corresponding data for proton-irradiated detectors are in agreement with these results [13] .

The comparison between the 0°C and room temperature reverse annealing suggests that in spite of a much higher initial change of the effective impurity concentration immediately after irradiation, and a considerable lengthening of the short-term annealing, the freezing of the long-term process is responsible for a pronounced net improvement. However, further investigations are necessary to prove this expectation.

In any realistic scenario for future collider experiments, the temperature at which the detectors will be operated has to be carefully optimized with respect to the different degradation

effects mentioned in Section 1. In general, the reverse current can be dramatically reduced at lower temperatures. On the other hand, such a reduction will probably have an adverse effect on the charge collection efficiency by the freezing of trapped charges. For irradiation and annealing at room temperature, with a subsequent charge collection measurement at 0°C, such an effect was shown to be negligible [14]. However, it could be much more significant in a situation where the detector is irradiated and kept at lower temperatures as is foreseen in the real operational scenario. With respect to the effective impurity concentration, one would have to fold the results shown in Fig. 7 with the neutron flux during operation. As the total operational time will be large, the short-term effects are completely washed out both for 20°C and 0°C. However, the long-term reverse annealing is apparently frozen at 0°C. Although a 10-year radiation-hardness test is clearly not feasible, it must nevertheless be demonstrated that silicon detectors can stand the consecutive cycles of damage and annealing during such an operational period. Following our results presented above, this proof can be achieved by compressing the time scale appreciably by using higher annealing temperatures. From the values of Table 2 we have for 10^{13} n/cm^2 a reverse annealing time constant of $t_{1/2}$ = 22 days at 50°C instead of 4.3 years at room temperature. We are therefore at present performing an experiment in which the detectors are irradiated with a given fluence once each month, and annealing is performed between exposures at a constant temperature of 50°C. The first results of this compressed scenario are shown in Fig. 8. From these experiments the cumulative change of the effective impurity concentration measured immediately before each exposure was plotted against the integrated fluence. Figure 9 gives the results which also include additional damage/annealing cycles not shown in Fig. 8. The dependence on the fluence is best represented by a straight line, and its slope varies only slightly for the two detector types being investigated [Fig. 9 (a): $\Delta N_{eff}/\Phi = 0.076 + 0.005$ and Fig. 9 (b): $\Delta N_{eff}/\Phi = 0.067 + 0.006$].

These very consistent results were then taken as a final justification for the simulation of a real operational 10-year scenario. Here we have chosen a detector operation at room temperature (T = 21°C), an initial effective impurity concentration of 5×10^{11} cm^{-3} (8 kΩ cm), exposures of 100 days per year, and fluences between 2×10^{12} and 1×10^{13} n/cm^2 for each exposure. As it has been shown that for such a scenario only the reverse annealing is relevant, the short-term annealing was neglected, and the reverse annealing calculated with the second-order approach, using the values of Table 2. The results are given in Fig. 10. For a detector thickness of 250 μm a cumulated fluence of 5×10^{13} n/cm^2 in 10 years would lead to an acceptable depletion voltage of only 125 V. From Fig. 7 we foresee that this increase will be even less if the operational temperature is decreased.

4 CONCLUSIONS

Although the experimental results presented do not cover in detail the total temperature range of interest yet, it can be clearly seen that the time dependence of the reverse annealing cannot be described by a single first-order process. In an isochronal annealing study we have observed two activation stages at 370 K and 440 K which could, in principle, be responsible for the measured reverse annealing, even at room temperature. This would suggest that the time dependence may be parametrized by the superposition of two exponentials. Here we have used an alternative parametrization describing a second-order process, which gives a consistent description with parameters independent of the fluence. The dependence on the temperature is

best represented by an activation energy of 1.33 eV. Using the parametrization of this model a compressed time scenario was designed for which the behaviour of the detectors was investigated in consecutive cycles of irradiation and annealing. The second-order model description was used to simulate the increase of the effective impurity concentration during 10 years of real LHC operation. It is expected that an accumulated fluence of 5×10^{13} n/cm^2 leads to an acceptable increase of the depletion voltage at room temperature, and that moderate cooling would even improve this performance.

Acknowledgements

The authors greatly appreciate extensive discussions with A. Clark, A. Chilingarov and R. Wunstorf. Financial support is acknowledged from the BMFT to the Dortmund and Hamburg groups under contracts 05 SDD52 P and 05 SHH 19I.

References

[l] T. Schulz et al., RD2 Collaboration, talk given at the 5th Topical Seminar on Experimental Apparatus for High Energy Particle Physics and Astrophysics, San Miniato, Italy, 1993, to be published in Nucl. Instrum. Methods.

[2] H.W. Kraner et al., Nucl. Instrum. Methods **A326** (1993) 350.

[3] E. Fretwurst et al., Nucl. Instrum. Methods **A326** (1993) 357.

[4] E. Barberis et al., Nucl. Instrum. Methods **A326** (1993) 373.

[5] F. Lemeilleur et al., Nucl. Phys. **B32**, Proc. Suppl. (1993) 415.

[6] K. Gill et al., Nucl. Instrum. Methods **A322** (1992) 177.

[7] R. Wunstorf, PhD thesis, Univ. Hamburg (1992), Internal Report DESY FHlK–92–01 (1992).

[8] H.J. Brede et al., Nucl. Instrum. Methods **A274** (1989) 332.

[9] E. Leon Florian and M. Tavlet, CERN/TIS 91–06 (1991).

[10] E. Fretwurst et al., Nucl. Instrum. Methods **A288** (1990) 1.

[11] H. Feick, diploma thesis, University of Hamburg, 1993.

[12] J.W. Corbett, Electron radiation damage in semiconductors and metals, *in* Solid State Physics, eds. F. Seitt and D. Turnbull, Academic Press, New York and London, 1966.

[13] H.J. Ziock et al., talk presented at the International Symposium on Development and Application of Semiconductor Tracking Detectors, Hiroshima, Japan, 1993.

[14] S. Bates et al., RD2 Collaboration, Nucl. Instrum. Methods **A337** (1993) 57.

Table 1

Parameters of detectors used, irradiation experiments, and annealing temperature

Detector	Type[a)]	Area (cm^2)	Thickness (μm)	N_{eff} (10^{11} cm^{-3})	Particle	Energy (MeV)	Φ_{eq} (10^{13} cm^{-2})	κ[b)]	T_{irr} (°C)	T_{ann} (°C)
901G16	SB	0.44	395	5.16	n	6.2	2.0	1.53	21	20–200
911G36	SB	0.44	391	5.01	n	6.2	2.9	1.53	–20	20–150
912G15	SB	0.44	392	5.38	n	6.2	3.1	1.53	21	21
912G16	SB	0.44	392	5.45	n	6.2	8.7	1.53	21	21
922G02	SB	0.44	393	5.03	n	6.2	2.1	1.53	21	60
922G04	SB	0.44	393	5.07	n	6.2	4.4	1.53	21	50
922G08	SB	0.44	393	5.08	n	6.2	4.4	1.53	21	40
932G36	SB	0.44	391	6.36	n	14.1	1.52	1.88	21	70
M04	IP	1.0	317	3.30	n	~ 1	12	1.08	~ 25	~ 25
M18	IP	1.0	309	4.13	p	24×10^3	7.0	0.93	~ 25	~ 25
UA2 ISI 104	IP	5.31	300	3.89	n	6.2	0.99	1.53	0	0
922G19	SB	0.44	393	5.96	n	14.1	0–5.5	1.88	21	50
922G23	SB	0.44	393	5.02	n	14.1	0–5.8	1.88	21	50
922G32	SB	0.44	393	4.89	n	14.1	0–4.9	1.88	21	50
922G37	SB	0.44	393	4.98	n	14.1	0–6.0	1.88	21	50
MUEA12	IP	0.25	312	3.61	n	14.1	0–5.7	1.88	21	50
MUEA14	IP	0.25	310	4.75	n	14.1	0–6.7	1.88	21	50
MUEA16	IP	0.25	295	1.38	n	14.1	0–5.1	1.88	21	50
MUEA17	IP	0.25	295	0.92	n	14.1	0–3.8	1.88	21	50

a) SB: surface barrier detectors [10];
IP: ion-implanted detectors fabricated by Micron Semiconductor Ltd., UK.

b) Hardness factor defined by: Φ_{eq} (1 MeV) = $\kappa \times \Phi$ (E) [3,7].

Table 2

Reverse-annealing parameters extracted from fits according to second-order process [see Eq. (4)]

Detector	Irradiation	T_{ann} (°C)	k (cm^3/s)	$N_{X,0}/\Phi_{eq}$ (10^{-2} cm^{-1})
932G36	neutron	70	$(2.6 \pm 0.2) \times 10^{-17}$	4.7 ± 0.1
922G02	neutron	60	$(6.8 \pm 0.8) \times 10^{-18}$	4.7 ± 0.1
922G04	neutron	50	$(1.2 \pm 0.1) \times 10^{-18}$	4.6 ± 0.1
922G08	neutron	40	$(4.9 \pm 0.5) \times 10^{-19}$	4.7 ± 0.1
912G15/16	neutron	21	$(1.3 \pm 0.6) \times 10^{-20}$	5.7 ± 0.2
M04	neutron	~ 25	$(2.1 \pm 0.1) \times 10^{-20}$	2.6 ± 0.1
M18	proton	~ 25	$(2.6 \pm 0.5) \times 10^{-20}$	4.3 ± 0.2

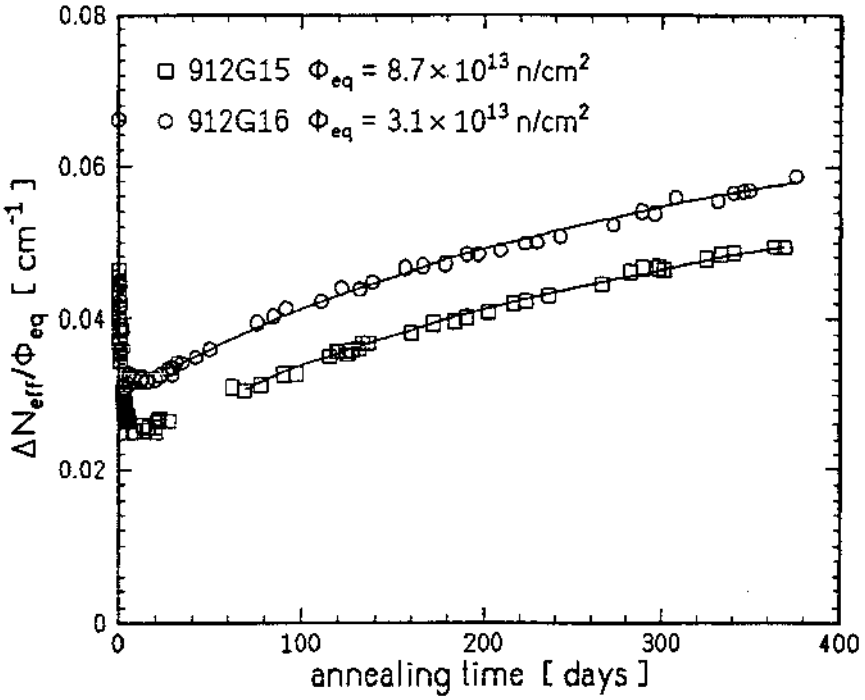

Fig. 1 Room temperature annealing of the change of the effective impurity concentration after neutron irradiation.

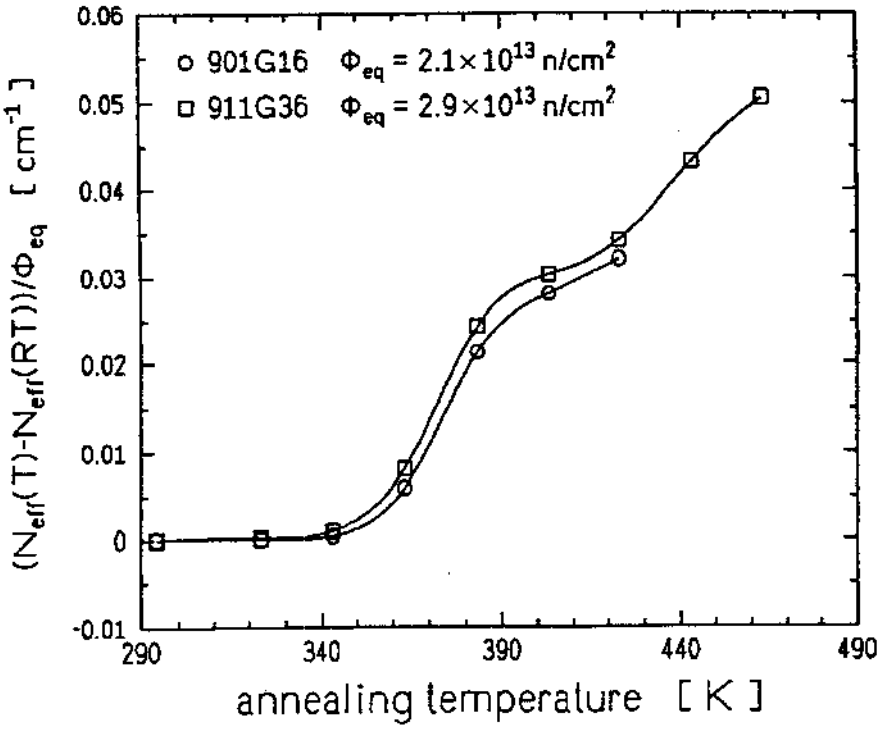

Fig. 2 Isochronal annealing of the effective impurity concentration with respect to N_{eff} at room temperature RT and normalized to Φ_{eq}.

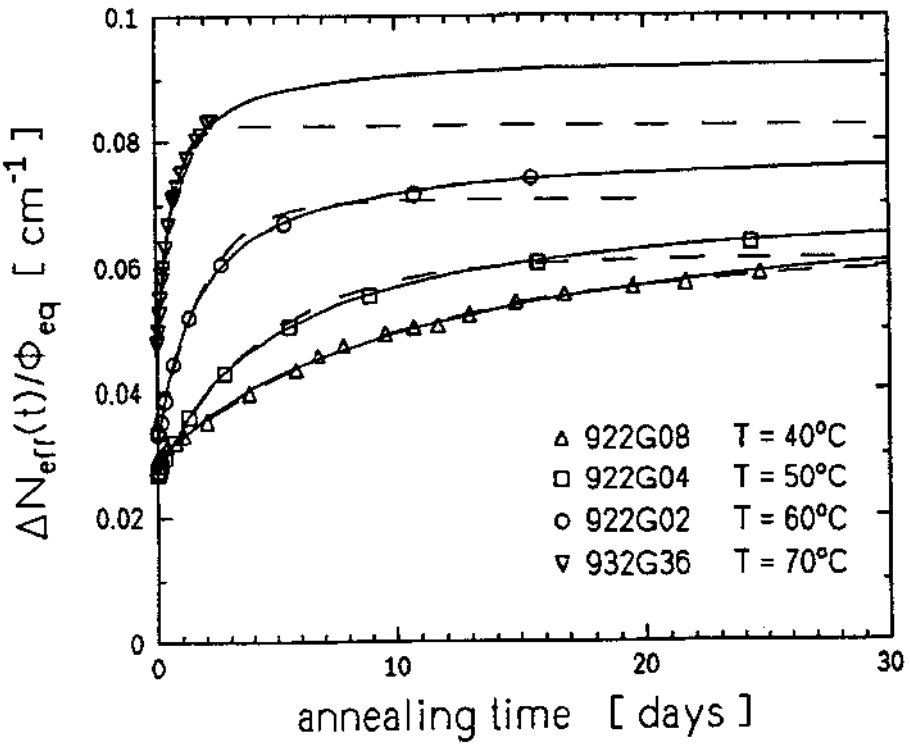

Fig. 3 Isothermal annealing of $\Delta N_{eff}/\Phi_{eq}$ (solid lines: second-order process, broken lines: first-order process).

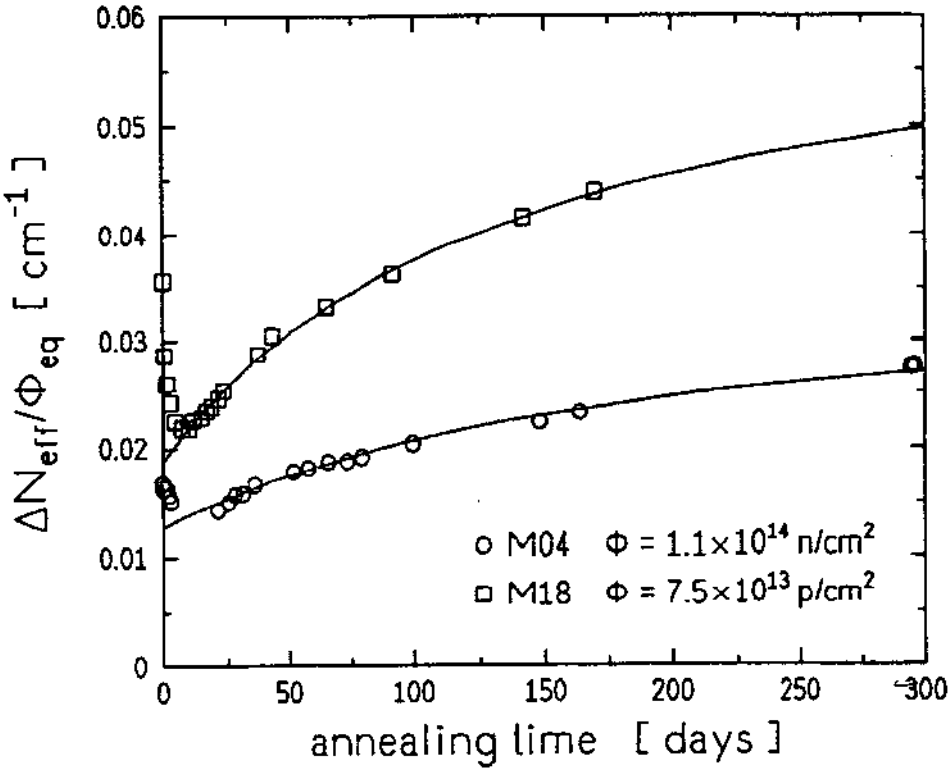

Fig. 4 Comparison of room temperature annealing of $\Delta N_{eff}/\Phi_{eq}$ after neutron and proton irradiation.

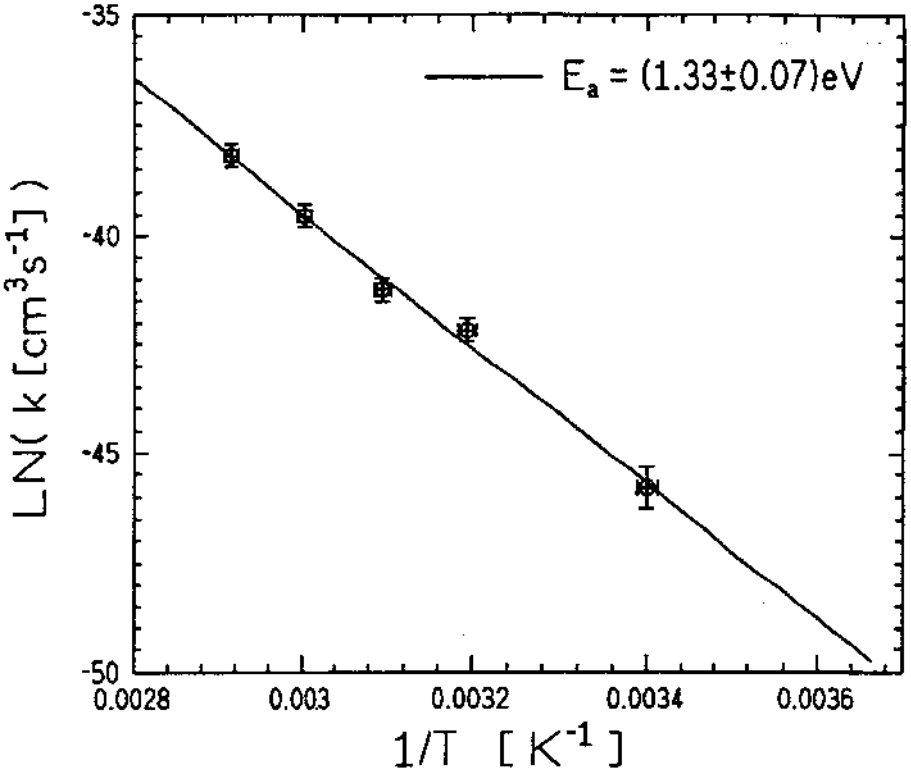

Fig. 5 Arrhenius plot of the rate constant k listed in Table 2.

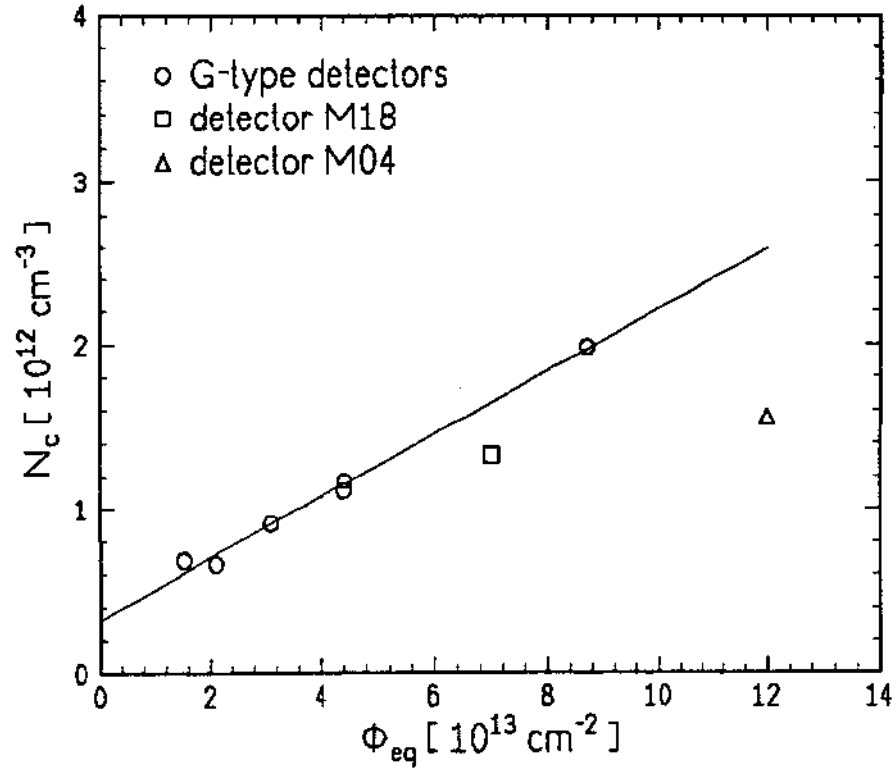

Fig. 6 The constant term N_C in Eq. (6) as a function of fluence (see text).

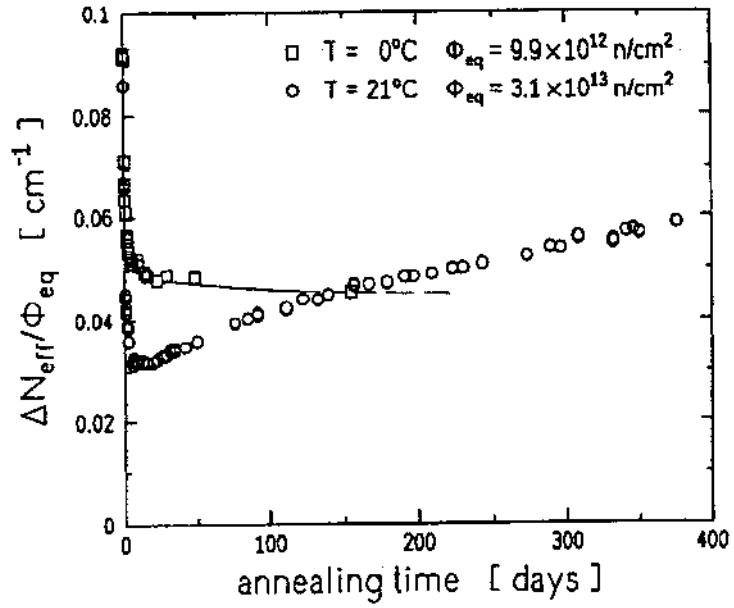

Fig. 7 Comparison of annealing behaviour at 0°C and room temperature.

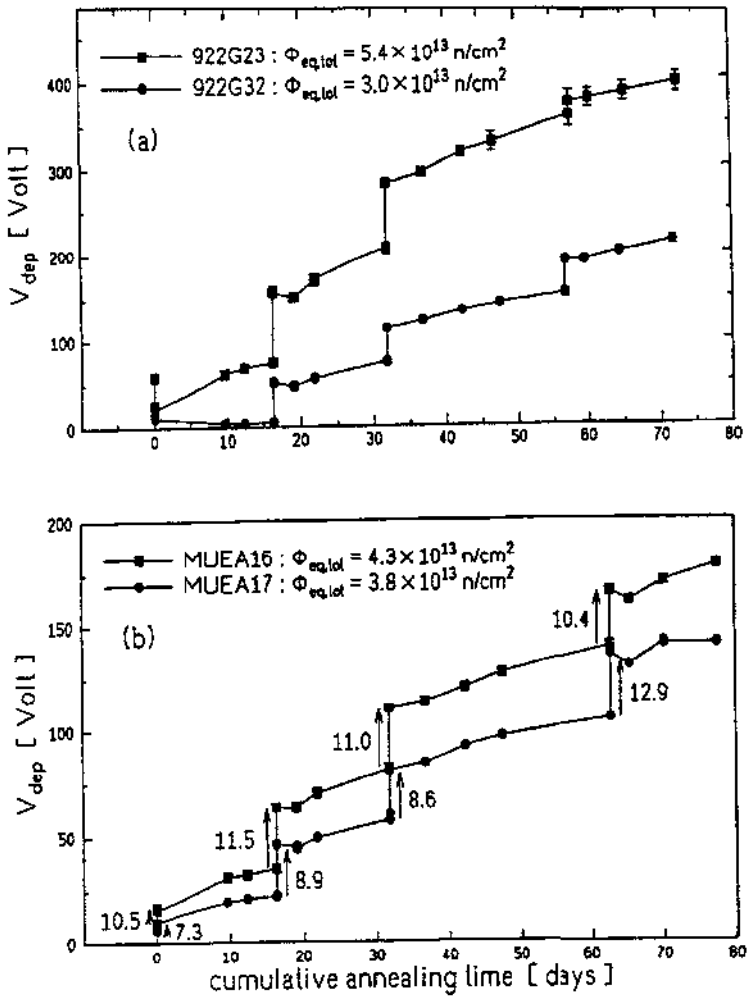

Fig. 8 Results of the first steps in the compressed time scale for different detector types: (a) surface barrier, and (b) ion implanted detectors. Irradiations are marked with arrows, and the numbers give the neutron fluence in units of 10^{12} n/cm^2.

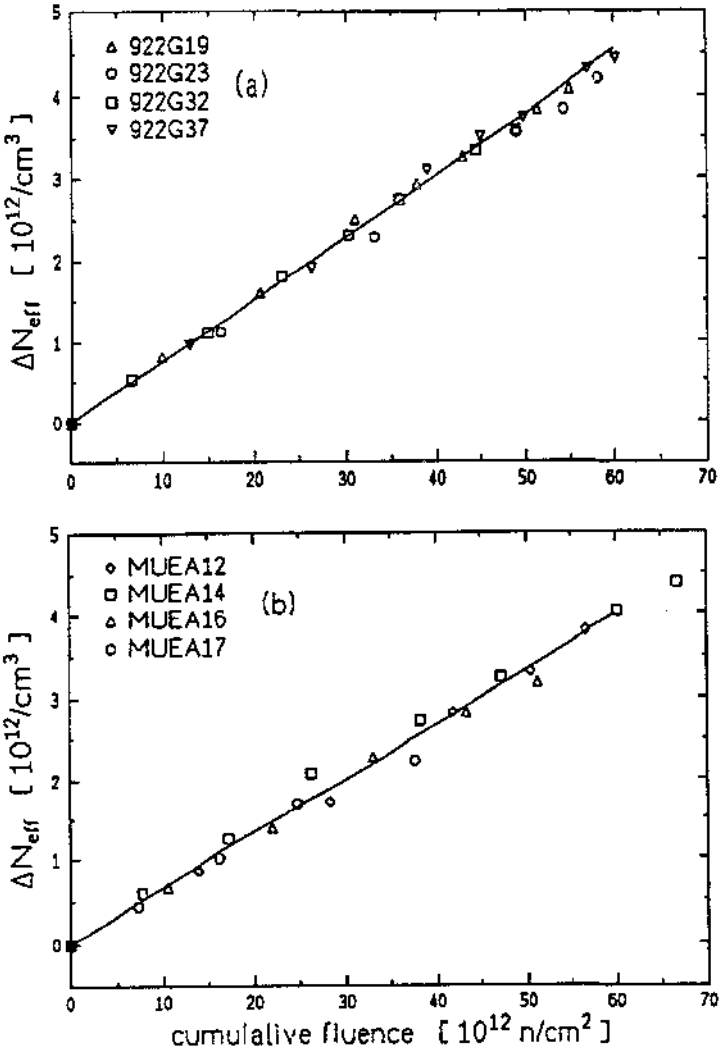

Fig. 9 Neutron-induced change of the effective impurity concentration for different detector types (as in Fig. 8), as a function of the cumulated fluence resulting from the experiment with the compressed time scale (see text).

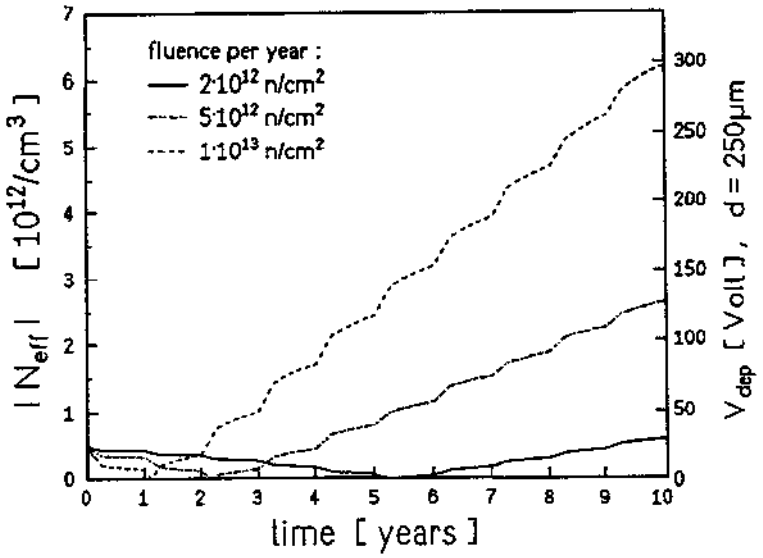

Fig. 10 Simulation of the time dependence of $|N_{eff}|$ and of the depletion voltage for ten years of operation at room temperature, with different fluences per year, using the second-order model for the reverse annealing.